Partial Alignment of Astrometric Position Excursions of International Celestial Reference Frame Quasars with Radio Jet Structures

Valeri V. Makarov, Phil Cigan, David Gordon, Megan C. Johnson, Christopher Dilullo, Sébastien Lambert

The Astrophysical Journal Letters, 977:L14 (6pp), 2024 December 10 https://doi.org/10.3847/2041-8213/ad94f1

Partial Alignment of Astrometric Position Excursions of International Celestial Reference Frame Quasars with Radio Jet Structures

Valeri V. Makarov[1], Phil Cigan[1], David Gordon[1], Megan C. Johnson[1], Christopher DiLullo[1,2], and Sébastien Lambert[3]
[1] U.S. Naval Observatory, 3450 Massachusetts Ave. NW, Washington, DC 20392-5420, USA; valeri.v.makarov.civ@us.navy.mil
[2] Computational Physics, Inc., 8001 Braddock Rd., Suite 210, Springfield, VA 22151, USA
[3] SYRTE, Observatoire de Paris, Université PSL, CNRS, Sorbonne Université, LNE, 61 avenue de l'Observatoire, 75014 Paris, France
Received 2024 October 31; revised 2024 November 16; accepted 2024 November 17; published 2024 December 3

Abstract

Published analyses of very long baseline interferometry data for the sources included in the third International Celestial Reference Frame catalog have revealed object-specific, excess astrometric variability and quasi-coherent trajectories as functions of time. A fraction of these sources show markedly elongated distributions of positions on the sky measured with diurnal observations. Here we apply a novel statistical and data-processing method to the diurnal position measurements stretching over 40 yr to quantify the degree of elongation and its position angle, for each source with more than 200 data points. We find that 49% of the examined sources have distribution elongations in excess of 1.3. Robust uncertainties of the directions of maximal astrometric dispersion are computed by the bootstrapping method, and the results are compared with a larger catalog of radio jet directions by A. V. Plavin et al. (2022). Nearly one-half of the sources with smaller position angle uncertainties are found to have astrometric position excursions from their mean positions aligned with the radio jet structures within $\pm 30^{\circ}$.

Unified Astronomy Thesaurus concepts: Very long baseline interferometry (1769); Astrometry (80); Radio loud quasars (1349); Radio jets (1347); Position angle (1286); Radio astrometry (1337)

Materials only available in the online version of record: machine-readable table

1. Introduction

Astrometric accuracy of Very Long Baseline Interferometry (VLBI) measurements and intrinsic positional stability of radio-loud quasars are of paramount importance for the temporal consistency and rigidity of the International Celestial Reference Frame (ICRF; C. Ma et al. 1998), which is currently adopted by the International Astronomical Union as the realization of the International Celestial Reference System (ICRS; e.g., E. F. Arias et al. 1995) at radio wavelengths. The latest version, ICRF3 (P. Charlot et al. 2020), adopted as the fundamental realization of the ICRS in 2019,[4] is defined not only in the previously utilized S/X bands (2.3/8.4 GHz, respectively), but also in the K and X/Ka bands (24 GHz and 8.4/32 GHz, respectively). The S/X catalog remains the largest and the most observed component, including over 5000 radio sources.[5] These distant extragalactic objects (radio-loud active galactic nuclei) have been assumed to be extremely compact and astrometrically stable sources of light. Evidence has been recently presented, however, that this is not true for some of these sources (O. Titov & S. Frey 2020; O. Titov et al. 2023). In a broader statistical study of more than 5500 radio sources (including 4536 ICRF3 objects), P. Cigan et al. (2024) found that practically all quasars with more than 200 single-epoch precision measurements show excessive dispersion around their long-term mean positions on the sky, which is not adequately represented by the available formal covariance. The position residuals do not follow the expected bivariate normal distribution. The sample distribution has powerful tails stretching well beyond the formal confidence limits. Furthermore, when the sequence of single-epoch positions is viewed as a time series, some of the well-observed sources show quasi-coherent trajectories upon suitable smoothing of the residuals.

The apparent astrometric instability of ICRF radio sources is probably related to the misalignment of individual positions as a function of wavelength, which becomes apparent when the VLBI-based astrometry is compared with the optical mean positions measured by the ESA Gaia mission (Gaia Collaboration et al. 2016). At the level of precision achieved so far on both sides, at least one-third of common radio-optical sources show statistically significant offsets outside the acceptable confidence levels (Y. Y. Kovalev et al. 2017; V. V. Makarov et al. 2017, 2019; L. Petrov & Y. Y. Kovalev 2017; J. Frouard et al. 2018; L. Petrov et al. 2019; N. Liu et al. 2020). Multiple, object-specific factors can contribute to this positional discrepancy on both the optical and radio sides. A significant fraction of the large radio-optical offsets was found to correlate with the directions of detected linear, jet-like radio features (Y. Y. Kovalev et al. 2017; L. Petrov et al. 2019; A. V. Plavin et al. 2019a), as well as with more generally evaluated radio source structures (M. H. Xu et al. 2021). The synchrotron opacity of the compact radio core can change on timescales from days to decades resulting in a so-called "core shift" variability (e.g., A. V. Plavin et al. 2019b) at the 0.1−1 mas level (K. V. Sokolovsky et al. 2011; A. B. Pushkarev et al. 2012).

In this Letter, we look at the problem of frequency-dependent and time-variable astrometric positions of ICRF3 sources from a different angle, employing the available single-epoch precision VLBI data to determine the position angles of the intrinsic wobbles on the sky. The general idea is related to

[4] https://www.iau.org/static/resolutions/IAU2018_ResolB2_English.pdf
[5] In the most recent USNO global solutions https://crf.usno.navy.mil/quarterly-vlbi-solution.

the previous work by C. Gattano & P. Charlot (2021), who demonstrated that the vectors of position offsets for each source are often (in more than half of the sample) not uniformly distributed in position angle. Some of the ICRF objects were found to present a single "preferred" direction of astrometric dispersion. However, the majority of these cases were found to be consistent with enhanced dispersion in the local south–north direction, i.e., in the decl. coordinate. The relative underperformance of VLBI astrometry in decl. is a fully expected consequence of the geometric configuration of the typical VLBI session networks and the intrinsic atmosphere calibration uncertainties. The baselines involved in each session are mostly east–west oriented, creating more favorable conditions to measure the R.A. coordinate component with higher precision. This geometric asymmetry should be captured by the formal covariance of each single-epoch position measurement, reflecting in the error ellipses elongated mostly in the south–north direction on the sky. Our goal is to find a method that is impervious to the expected stochastic asymmetry of single-epoch VLBI astrometry, allowing us to reveal the physical orientation of apparent position excursions.

2. Data

We use a data set of diurnal VLBI sessions spanning over 40 yr of continued observations with the global International VLBI Service for Geodesy and Astrometry (IVS) and VLBA networks. The data are taken from the usn2023a USNO global solution, which is described in more detail by P. Cigan et al. (2024). The principles of the VLBI global solutions can be found in A. de Witt et al. (2022). The standard simultaneous S/X band setup is utilized, where the S-band (2.3 GHz) is used for determining the ionosphere contribution to the delay and improving the final solution defined at 8.4 GHz in the X-band. The usn2023a solution provides a time sequence of individual (R.A., decl.) coordinates for each single session of VLBI measurements, which nominally correspond to 1 day. Each source has a number of individual position determinations ranging from a few to a few thousand for the most frequently observed objects. The mean positions over the entire span of VLBI observations can be computed and compared with the mean positions tabulated in the ICRF3 S/X catalog.

The input data for this analysis are the time series from 6581 of these diurnal sessions. Each data point is a tuple of R.A. and decl. coordinates, which are defined in the ICRF3. The coordinates have three associated formal covariance parameters, including the standard errors (uncertainties) in milliarcseconds and the correlation coefficient. Closely following the procedure described in P. Cigan et al. (2024), we start by computing the mean position for each source using the maximum likelihood (ML) principle and assume that the coordinate measurements are normally distributed with the specified covariances. The residual offset vectors are then computed for each session and each source by subtracting the mean positions computed in the ML framework. For practical convenience, these offset vectors are called $[x, y]^T$ here, denoting the local residuals $\Delta\alpha \cos\delta$ and $\Delta\delta$, respectively. The corresponding formal covariance matrix is designated as $\boldsymbol{C}_{xy}$.

Our analysis is further restricted to 265 ICRF3 sources with at least 200 individual observing sessions each. This filter is driven by the required number statistics to obtain a reliable determination of possible asymmetry in the scatter of individual offsets. Approximately half of the selected objects are defining ICRF3 sources, which represent the backbone of this celestial frame because they are internally used to align and calibrate the global VLBI solutions. The number of measurements is uneven among the 265 sources, with some of them counting up to a few thousand data points.

3. Method

Our method uses the standardized offset vector

$$\boldsymbol{u} \equiv [u_x, u_y]^T = \boldsymbol{C}_{xy}^{-\frac{1}{2}} [x, y]^T, \quad (1)$$

which is expected to follow a bivariate normal distribution of unit variance and zero correlation. In reality, these vectors invariably show excess dispersion for sources with more than 200 measurements, which we have interpreted as evidence for genuine stochastic trajectories of ICRF quasars (or "cosmic error"). However, this operation helps to remove most of the technical distortion in the sample distribution of residuals related to the predictable covariances of coordinate measurements. An example of such improvement is shown in Figure 1. The left panel is the scatterplot of the VLBI measured position offsets $\{x, y\}$ for the ICRF3 quasar IERS B1334−127, which is one of the most-observed sources with 3174 single-epoch determinations in our database. The cloud of points is conspicuously elongated in the S–N direction, possibly with a small tilt. This shape is consistent with the formal covariances, which indicate larger uncertainties in the decl. component due to the configurations of VLBI baselines. The right plot displays the distribution of standardized $\boldsymbol{u}$ endpoints according to Equation (1). This distribution is much more rotation-symmetric without any obvious direction of enhanced dispersion. Thus, in this case, the standardization effectively removes the technical deformation of position excursions, which is not related to the physics of the object.

In P. Cigan et al. (2024), the normalized single-epoch position offset,

$$D = \sqrt{[x, y]\, \boldsymbol{C}_{xy}^{-1}\, [x, y]^T} = \sqrt{\boldsymbol{u}^T\, \boldsymbol{u}}, \quad (2)$$

and the related dimensionless score parameter, $Q68$, which is the 68th percentile of the D sample, were used to quantify the magnitude of the excessive dispersion. Here, we compute a different quantity, which is the position angle ϑ of the long axis of the possible remaining elongation of the standardized residuals $\boldsymbol{u}$, from the local north (y) direction.

The observed distributions of standardized offsets are often non-Gaussian and show a variety of shapes. One possible approach would be to fit a common functional form with free parameters for each source. The bivariate Student T distribution could be a reasonable choice because it runs the gamut of heavy-tailed functions from Normal to Cauchy types depending on the fitted number of degrees of freedom. In this study, we chose an alternative nonparametric approach, which avoids possible systematic errors due to a mismatch of the model distribution. We compute the empirical distribution function of $\boldsymbol{u}$ for each source using Wolfram Mathematica's *EmpiricalDistribution* function.[6] The cumulative distribution function (CDF) is represented by a step function counting the number of

[6] https://reference.wolfram.com/language/ref/EmpiricalDistribution.html

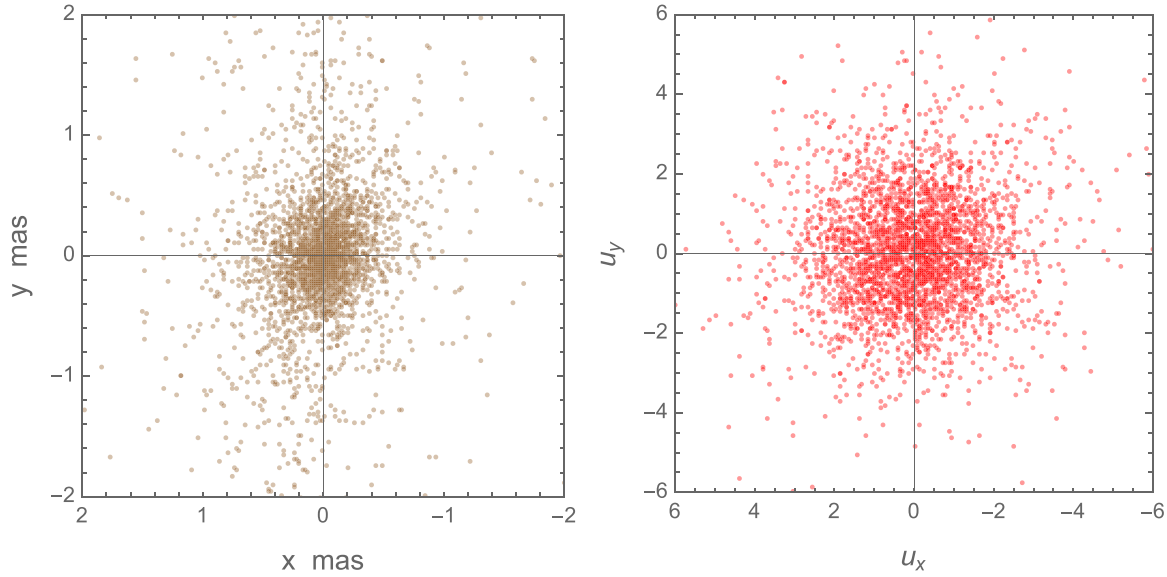

Figure 1. VLBI-measured position offsets of the ICRF3 source IERS B1334−127 with respect to its maximum-likelihood mean position. Left: offsets in tangential sky coordinates x (R.A.) and y (decl.) in milliarcseconds. Right: standardized offsets $\{u_x, u_y\}$ (Equation (1)) relative to the same mean position.

instances below the argument point. This is a sufficiently accurate (but discretized) representation of the CDF for a large sample. The emerging CDF can be used to compute the probability density function, moments (including the mean), and the 2-by-2 covariance matrix. The latter contains the information about the confidence areas (ellipses) that we need for this analysis.

If $\boldsymbol{C}_u$ is the empirical covariance matrix of the sample distribution of $\boldsymbol{u}$ for a given source, its eigenvectors $\boldsymbol{e}_1$ and $\boldsymbol{e}_2$ and the respective eigenvalues ϵ_1 and ϵ_2 can be directly computed. An elongated distribution along a certain direction is evident as $\epsilon_1/\epsilon_2 > 1$, in which case the position angle of the vector $\boldsymbol{e}_1 \equiv [e_{1x}, e_{1y}]^T$ defines this preferred direction. Thus, we compute the degree of elongation

$$\varepsilon = \epsilon_1/\epsilon_2, \tag{3}$$

and the position angle of the major axis of the confidence ellipse by[7]

$$\vartheta = \arctan(e_{1y}, e_{1x}). \tag{4}$$

This furnishes the angle in accordance with the astronomical convention, where it is rendered from the local north direction through east. However, due to the axial symmetry of the confidence ellipse, this direction is modulo-π invariant. The emerging negative values of ϑ are redefined to the support interval [0°, 180°] by adding 180°.

While this calculation is relatively straightforward, it is also important to estimate the associated uncertainties. Here, in the spirit of robust statistical analysis, we use the bootstrapping method. For each source, we perform 3000 trial computations of $\boldsymbol{e}_1$, $\boldsymbol{e}_2$, ε, and ϑ for randomly selected (without repetition) subsets of data points including half of the entire sample. Robust estimates of the uncertainties of ε, and ϑ are computed as the difference of 0.84- and 0.16-quantiles of the bootstrapped sample distributions divided by $2\sqrt{2}$. The latter coefficient factors in the expected loss of precision due to the halving of the available data set. The resulting robust uncertainties are denominated σ_ε and σ_ϑ.

[7] Note that in the adopted Wolfram's notation, the two-argument arctan(x, y) corresponds to arctan(y/x), i.e., the arguments are swapped.

4. Results

The computed position angles of the greatest dispersion in $\boldsymbol{u}$ for 265 ICRF quasars are fairly uniform in the interval [0°, 180°] with a moderate enhancement at $P \simeq 90°$. This enhancement is likely to be the remaining artifact of the VLBI astrometry technique. The dominant orientation of the VLBI baselines in the east–west direction on the surface of Earth results in a considerably better formal precision of the measured R.A. components. The cosmic error is assumed to be isotropic, but it shows more clearly in R.A. because of the smaller formal uncertainties. We are, however, mostly interested in a subset of the 265 sources, where the angle uncertainties are small enough and the elongation ε is large enough for a meaningful comparison with imaging data.

We find that the majority of the initial sample has moderate elongation estimates ε, with 49% of the sample ϵ exceeding 1.3, and 29% above 1.5. Reliable estimates can only be obtained for objects with significant elongations of $\boldsymbol{u}$-distributions. The standard errors σ_ϑ, which quantify the robustly estimated internal precision of ϑ, are smaller than 5° for 25% of the sample, and smaller than 10° for 53% of the sample. We note that a large σ_ϑ value does not necessarily signify a stable, astrometrically fixed source, but rather, the absence of a specific direction of position walks. Table 1 shows the leading 10 entries of the output table with the derived parameters. The entire data sample for 265 ICRF sources is available.

The greatest elongation $\epsilon = 5.43$ is found for IVS B1038+52A = ICRF J104146.7+523328 = SDSS J104146.77+523328.2. The cloud plots of $\{x, y\}$ and $\boldsymbol{u}$ offsets similar to Figure 1 (not displayed here for brevity) both show extremely elongated configuration, even suggesting a dual source with a ∼1.5 mas separation. The computed orientation $\vartheta = 16\overset{\circ}{.}2 \pm 1\overset{\circ}{.}4$ determined in this study is consistent with the position angle of the jet structure clearly visible in high-resolution hybrid VLBI-maps (M. J. Rioja et al. 1997). The reported ibid. changes in the separation between the sources A

Table 1
Directions of Preferred Astrometric Walks for 265 ICRF3 Quasars

IERS name	Mean R.A. (deg)	Mean decl. (deg)	ϑ (deg)	σ_ϑ (deg)	ε	σ_ε
(1)	(2)	(3)	(4)	(5)	(6)	(7)
0003-066	1.557887101	−6.393148984	170.5	12.9	1.11	0.044
0008-264	2.755194559	−26.209271393	117.1	20.2	1.282	0.122
0014+813	4.285310567	81.58559331	177.7	1.2	3.448	0.249
0016+731	4.940777101	73.458337975	97.7	1.4	3.051	0.166
0017+200	4.907726976	20.362679197	79.7	32.6	1.109	0.08
0019+058	5.635171635	6.134519947	93.	38.6	1.076	0.075
0048-097	12.672155741	−9.484781904	80.9	15.2	1.089	0.043
0048-427	12.78959093	−42.442581219	146.8	18.2	1.366	0.211
0059+581	15.690676528	58.40309348	119.4	34.3	1.021	0.026
0104-408	16.687948563	−40.572211249	135.2	14.8	1.109	0.052

Note. IERS name in column (1) is obtained by prepending IERS B to the given code. R.A. and decl. coordinates in columns (2) and (3) are the VLBI mean coordinates. Position angles of preferred astrometric walks ϑ in column (4) are computed per Equation (4), and the elongation parameters ε in column (6) per Equation (3) (see Section 3).

(This table is available in its entirety in machine-readable form in the online article.)

and B, which are unrelated quasars 33″ apart, are undoubtedly caused by the walks of the A source, because of the aligned A–B position angle. The time evolution of the single-epoch positions clearly shows a coherent transition northward along ϑ over approximately 12 yr, illustrated in Figure 2.

5. Comparison with Radio Jet Directions

We use the results by A. V. Plavin et al. (2022) to compare the directions of astrometrically detected walks with position angles of radio jet structures. The input catalog includes 9220 entries, of which 228 match the objects in our working sample. The formal precision of radio jet position angles $\vartheta_{\rm jet}$ is mostly higher (peaking at ∼3°) than our robustly estimated precision of $\vartheta_{\rm ast}$. Therefore, we further limit this comparison to 127 ICRF sources with $\sigma_\vartheta < 10°$ from our analysis. The jet directions are estimated on the full support interval [−180°, 180°], while our elongation directions are modulo-π indeterminate. We mirrored the jet position angles by adding 180° to all negative values.

The histogram of computed $\vartheta_{\rm ast} - \vartheta_{\rm jet}$ is reproduced in Figure 3. The expected distribution of differences in position angles for isotropic, statistically independent samples is triangular, as shown with the orange line normalized to the total number of points and the 5° bin. The strongly bell-shaped histogram peaked around 0 indicates that a considerable fraction of VLBI sources are well-aligned with the independently estimated jet directions. Note that a few sources with P.A. differences close to ±180° are also the aligned cases because those were separated in the plot by the modulo-π adjustment.

Counting all cases in excess of the expected distribution within the interval [−30°, +30°], we estimate that nearly half of this selection has aligned directions. A slightly higher rate of alignments is found when the sample is further limited to $\epsilon > 1.1$ cases. On the other end of the range, a number of sources are obviously present with significant deviations of the preferred astrometric walks from the radio jet direction. We find 10 sources, for example, with $\vartheta_{\rm ast} - \vartheta_{\rm jet}$ in excess of 45°, which have elongations $\epsilon > 1.5$ and formal errors $\sigma_\vartheta < 10°$, although two of them are cases of the 180° split. The most confidently detected case of misalignment is the blazar B2229+695, which shows a distinct quasi-coherent astrometric

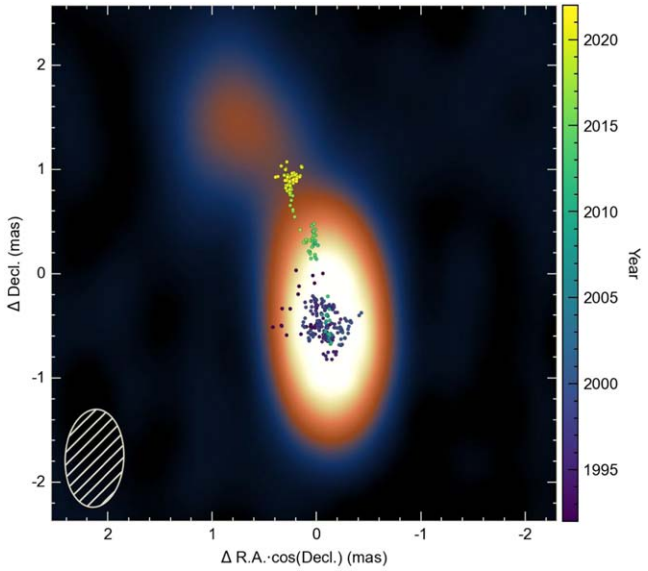

Figure 2. *X*-band image of B1038+52A from USNO's FRIDA database (https://crf.usno.navy.mil/FRIDA), observed on 2008 January 23. The hatched ellipse denotes the beam FWHM. The astrometric measurements, smoothed over a rolling 4 month time window as described in P. Cigan et al. (2024) to enhance the visibility of coherent trends, are overlaid as scatter points colored by time.

trajectory in R.A. The jet direction from A. V. Plavin et al. (2022) is 43 ± 5°, while our robust determination is 89.°0 ± 0.°9. We note, however, that the estimated core-jet shift is 2.6 mas, which is much greater than the typical astrometric excursion in R.A. within 1 mas. A small fraction of VLBI measurements show extreme outliers separated by ∼2 mas and more from the mean position, whose location is more consistent with position angle (PA) ≃ 45°.

The low-spectral peaked quasar 0607-157 (PKS 0607-15) exhibits a northeastward extension of the jet (MOJAVE 15 GHz observations suggest a stationary knot around 17 mas from the radio core; M. L. Lister et al. 2018; illustrated here in Figure 4), while the inner structure within 2 mas from the core indicates rather eastward ejections. A. V. Plavin et al. (2022) found jet directions averaging 38 ± 5° across several bands, with the lowest frequencies consistent with the 17 mas extension. Our

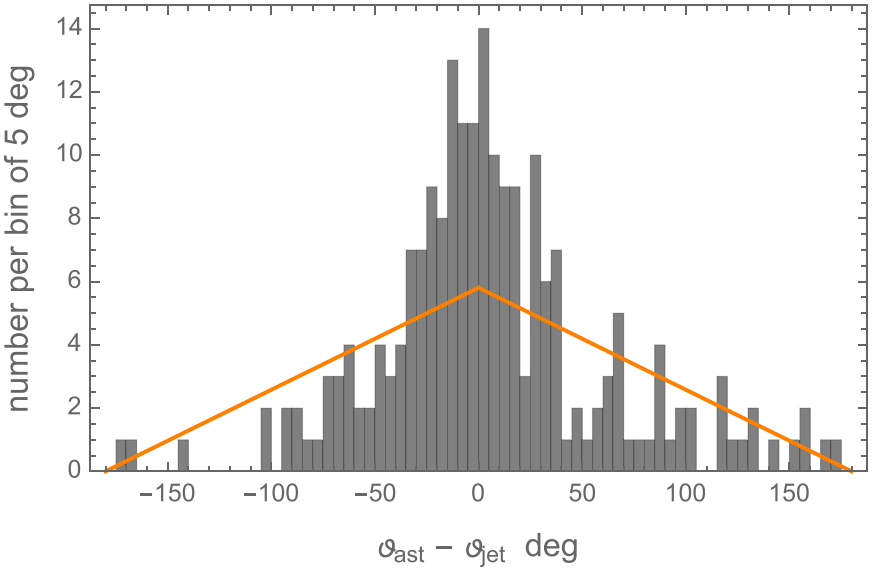

Figure 3. Histogram of differences between the position angles of preferred astrometric excursions determined in this Letter ($\vartheta_{\rm ast}$) and the position angles of radio jets ($\vartheta_{\rm jet}$) from A. V. Plavin et al. (2022), modulo π.

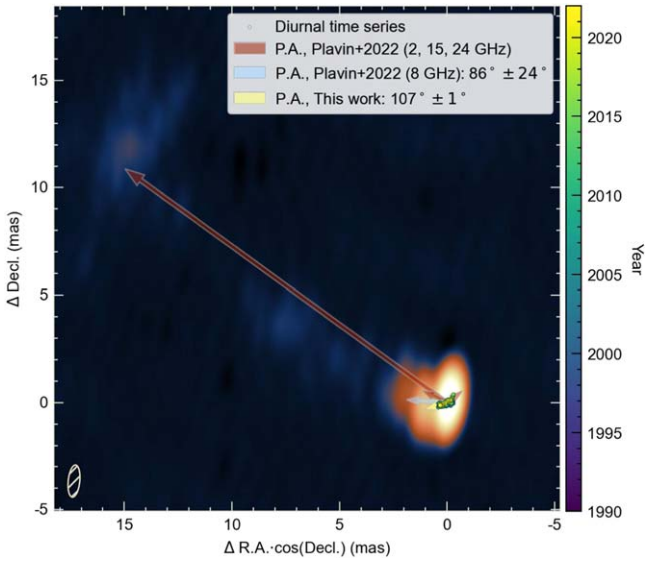

Figure 4. A 15 GHz MOJAVE image of 0607−157 (M. L. Lister et al. 2018), clearly showing emission in multiple extended regions. The scatter points are the astrometric time series, colored by time, and are smoothed over a rolling 4 month time window as described in P. Cigan et al. (2024). The red arrows correspond to the jet angles and median distances determined by A. V. Plavin et al. (2022) at various frequencies, and the blue arrow corresponds to the same at 8 GHz. The yellow arrow denotes the angle of preferred astrometric excursion $\vartheta_{\rm ast}$.

determination is $107 \pm 1°$. The difference between the two estimates suggests that our determination is more sensitive to the regions close to the VLBI centroid—that is, in the case of 0607−157, the radio core (base of the jet)—while A. V. Plavin et al. (2022) estimates may be more influenced by the extended regions. Though the difference can be small for straight jets, it becomes strongly separation-dependent for curved jets. We also note the wide range of wavelength-specific determinations of jet directions and core-jet distances in A. V. Plavin et al. (2022) for this object ranging from 50° (17.2 mas) at 1.4 GHz to −64° (0.3 mas) at 43 GHz. Their 86° (1.3 mas) determination at 8 GHz is rather close to our astrometric data in the *X*-band in both the PA and linear extent.

We find that the absolute difference in position angle $\vartheta_{\rm ast} - \vartheta_{\rm jet}$ appears to be significantly correlated with the viewing angle on the line of sight, the latter being available from D. C. Homan et al. (2021) for 110 sources in our sample. Spearman's ρ is −0.24 with $p = 0.011$ for this correlation, suggesting that, on average, small viewing angles are more often associated with greater $|\vartheta_{\rm ast} - \vartheta_{\rm jet}|$ differences. For instance, 0607−157 has a viewing angle of 0.06°. Jets with small viewing angles (i.e., well-aligned with the line of sight) generate statistically smaller astrometric excursions with a more isotropic distribution around the mean position. Both effects randomize the estimated position angles $\vartheta_{\rm ast}$. This interpretation finds support in the negative correlation between $|\vartheta_{\rm ast} - \vartheta_{\rm jet}|$ and ε of −0.26 ($p < 0.001$), meaning that a small elongation is associated with worse alignment in PA.

6. Discussion and Future Work

The previous analysis of ICRF sources' position differences at three different radio wavelengths and in the optical (S. Lambert et al. 2021) supported the simple "core-jet" model, where the respective photocenters are well aligned with the dominant radio jet structure, but have systematic shifts along the jet. This study furnishes additional evidence that the intrinsic positional variability of ICRF sources within the single *X* band is often (but not always) correlated with the directions of the jets. Assuming that the projected jets are isotropic on the sky, the cosmic error component has a nonuniform impact on the stability and accuracy of the reference frame depending on specific applications. For example, the closely related Earth orientation determination and UT1−UTC monitoring are more sensitive to the R.A. component of reference sources' walks. Specific ICRF3 sources with significant elongations ε and position angles ϑ closer to 90° should be downweighted in such solutions. The impact of anisotropic excursions on geodetic nutation series can also be predicted by means of more sophisticated modeling (S. B. Lambert et al. 2008).

Our results confirm that the alignment of astrometric walks with jet structures is not universal. A significant fraction of investigated objects show a mismatch by more than 30°, which is

significant with respect to the estimated uncertainty. A. Moór et al. (2011) have detected this partial misalignment comparing the jet structures with ad hoc "proper motions" of a relatively small sample. Noting that the notion of quasar proper motions based on coordinate time series is somewhat dubious, given the stochastic character of the process, we do find more evidence here that some of the ICRF quasars are not compliant with the "core-jet" paradigm. For the example of B2229+695, we have seen a case of possible hierarchical stricture, where two different processes may be responsible for the variation of apparent position, on two angular scales <1 mas and $\geqslant 2$ mas. A possible explanation could also be found in the inverse correlation of the radio-optical position offsets with the degree of optical flux variability (N. J. Secrest 2022; S. Lambert et al. 2024), which is interpreted as the consequence of the line-of-sight alignment of relativistic jets in blazars and other highly variable sources. Future studies can therefore take different paths. On one side, a better characterization of astrometric radio sources with large elongation ϵ is warranted, including high-resolution imaging with VLBI in different bands, if possible. The other direction of future research would concern the noncompliant sources. Are they characterized by lower degrees of optical or radio variability? Do they have prominent one-sided jets? Can any evidence be found that these jets, if they are present, rapidly change their direction on the timescale of decades?

Acknowledgments

This work supports USNO's ongoing research into the celestial reference frame and geodesy. The National Radio Astronomy Observatory is a facility of the National Science Foundation operated under cooperative agreement by Associated Universities, Inc. The authors acknowledge the use of the Very Long Baseline Array under the U.S. Naval Observatory's time allocation. This research has made use of data from the MOJAVE database that is maintained by the MOJAVE team (M. L. Lister et al. 2018). The authors have used the IVS data archive maintained by the International VLBI Service for Geodesy and Astronomy, https://ivscc.gsfc.nasa.gov/products-data/index.html.

Facility: VLBA.

Software: `Mathematica` (Wolfram Research 2024).

ORCID iDs

Valeri V. Makarov https://orcid.org/0000-0003-2336-7887
Phil Cigan https://orcid.org/0000-0002-8736-2463
David Gordon https://orcid.org/0000-0001-8009-995X
Megan C. Johnson https://orcid.org/0000-0002-4146-1618
Christopher DiLullo https://orcid.org/0000-0001-5944-9118
Sébastien Lambert https://orcid.org/0000-0001-6759-5502

References

Arias, E. F., Charlot, P., Feissel, M., & Lestrade, J. F. 1995, A&A, 303, 604
Charlot, P., Jacobs, C. S., Gordon, D., et al. 2020, A&A, 644, A159
Cigan, P., Makarov, V., Secrest, N., et al. 2024, ApJS, 274, 28
de Witt, A., Charlot, P., Gordon, D., & Jacobs, C. S. 2022, Univ, 8, 374
Frouard, J., Johnson, M. C., Fey, A., Makarov, V. V., & Dorland, B. N. 2018, AJ, 155, 229
Gaia Collaboration, Prusti, T., de Bruijne, J. H. J., et al. 2016, A&A, 595, A1
Gattano, C., & Charlot, P. 2021, A&A, 648, A125
Homan, D. C., Cohen, M. H., Hovatta, T., et al. 2021, ApJ, 923, 67
Kovalev, Y. Y., Petrov, L., & Plavin, A. V. 2017, A&A, 598, L1
Lambert, S., Liu, N., Arias, E. F., et al. 2021, A&A, 651, A64
Lambert, S., Sol, H., & Pierron, A. 2024, A&A, 684, A202
Lambert, S. B., Dehant, V., & Gontier, A. M. 2008, A&A, 481, 535
Lister, M. L., Aller, M. F., Aller, H. D., et al. 2018, ApJS, 234, 12
Liu, N., Lambert, S. B., Zhu, Z., & Liu, J. C. 2020, A&A, 634, A28
Ma, C., Arias, E. F., Eubanks, T. M., et al. 1998, AJ, 116, 516
Makarov, V. V., Berghea, C. T., Frouard, J., Fey, A., & Schmitt, H. R. 2019, ApJ, 873, 132
Makarov, V. V., Frouard, J., Berghea, C. T., et al. 2017, ApJL, 835, L30
Moór, A., Frey, S., Lambert, S. B., Titov, O. A., & Bakos, J. 2011, AJ, 141, 178
Petrov, L., & Kovalev, Y. Y. 2017, MNRAS, 467, L71
Petrov, L., Kovalev, Y. Y., & Plavin, A. V. 2019, MNRAS, 482, 3023
Plavin, A. V., Kovalev, Y. Y., & Petrov, L. Y. 2019a, ApJ, 871, 143
Plavin, A. V., Kovalev, Y. Y., Pushkarev, A. B., & Lobanov, A. P. 2019b, MNRAS, 485, 1822
Plavin, A. V., Kovalev, Y. Y., & Pushkarev, A. B. 2022, ApJS, 260, 4
Pushkarev, A. B., Hovatta, T., Kovalev, Y. Y., et al. 2012, A&A, 545, A113
Rioja, M. J., Marcaide, J. M., Elosegui, P., & Shapiro, I. I. 1997, A&A, 325, 383
Secrest, N. J. 2022, ApJL, 939, L32
Sokolovsky, K. V., Kovalev, Y. Y., Pushkarev, A. B., & Lobanov, A. P. 2011, A&A, 532, A38
Titov, O., & Frey, S. 2020, RNAAS, 4, 108
Titov, O., Frey, S., Melnikov, A., et al. 2023, AJ, 165, 69
Wolfram Research, Inc 2024, Mathematica, v14.0, https://www.wolfram.com/mathematica
Xu, M. H., Lunz, S., Anderson, J. M., et al. 2021, A&A, 647, A189